Supporting Information

Metal-organic frameworks derived Cu nanoparticles binder-free monolithic electrodes with multiple support structures for electrocatalytic nitrate reduction to ammonia

Yingying Wang, [§] Yue Cao, [§] Yan Hai, Xinyan Wang, Senda Su, Wenming Ding, Zhenyu Liu, Xiaoman Li, and Min Luo*

State Key Laboratory of High-efficiency Utilization of Coal and Green Chemical Engineering, School of Chemistry and Chemical Engineering, Ningxia University, Yinchuan, Ningxia 750021, P. R. China

[§]These authors contributed equally to this work.

E-mail: luominjy@nxu.edu.cn

Contents

1. Experimental section

1.1 Determination of NO_3^--N

First, remove 1 mL electrolyte from the electrolytic cell and dilute it to 50 mL to the detection range. Afterwards, 1 mL 1 M HCl and 1 mL 0.8 wt% H_3NO_3S solution were added to the above solution. The absorbance was detected by UV-Vis spectrophotometry after 60 minutes at a wavelength of 220 nm and 275 nm. The final absorbance of NO_3^- can be calculated as following: $A=A_{220 nm} - 2A_{275 nm}$. The calibration curve can be acquired through different concentrations of KNO_3 solutions and corresponding absorbance. The fitting curve (y = 0.23994x + 0.02701, R^2 = 0.9991) exhibits great linear relation of absorbance value with NO_3^--N concentration.

Figure S1. (a) UV-Vis absorption curves of NO_3^--N. (b) Calibration curve used to estimate the concentrations of NO_3^--N.

1.2 Determination of NO_2^--N

A mixture of p-aminobenzenesulfonamide (5 g), HCl (50 mL), and ultrapure water (450 mL) were used as a color reagent. 1 mL electrolyte was extracted from the electrolytic cell and diluted to 100 mL to detection range. 1 mL mixed solution of p-aminobenzenesulfonamide and HCl and 1 mL N-(1-Naphthyl) ethylenediamine dihydrochloride (1 g/L) were added into the above solution and mixed uniformity. After standing at room temperature for 60 min, the absorbance was recorded at a wavelength of 540 nm. The concentration-absorbance curve was calibrated using the standard KNO_2 with different NO_2-N concentrations. The fitting curve (y = 3.4212x + 0.0001026, R^2 = 0.9998) exhibits great linear relation of absorbance value with NO_2^--N concentration.

Figure S2. (a) UV-Vis absorption curves of NO_2^--N. (b) Calibration curve used to estimate the concentrations of NO_2^--N.

1.3 Determination of NH₃-N

The Nessler's reagent was employed as the color reagent for the determination of NH_3-N. Firstly, 1 mL electrolyte was extracted from the cathodic chamber and diluted to 100 mL to detection range. Then, 1 mL of potassium sodium tartrate solution and 1 mL Nessler's reagent were subsequently added into the above solution and mixed uniformity. After standing at room temperature for 20 min, the absorbance was recorded at a wavelength of 420 nm. The concentration-absorbance curve was calibrated using the standard NH_4Cl with different NH_4^--N concentrations. The fitting curve (y = 0.1521x + 0.010, R^2 = 0.999) exhibits great linear relation of absorbance value with NO_4^--N concentration.
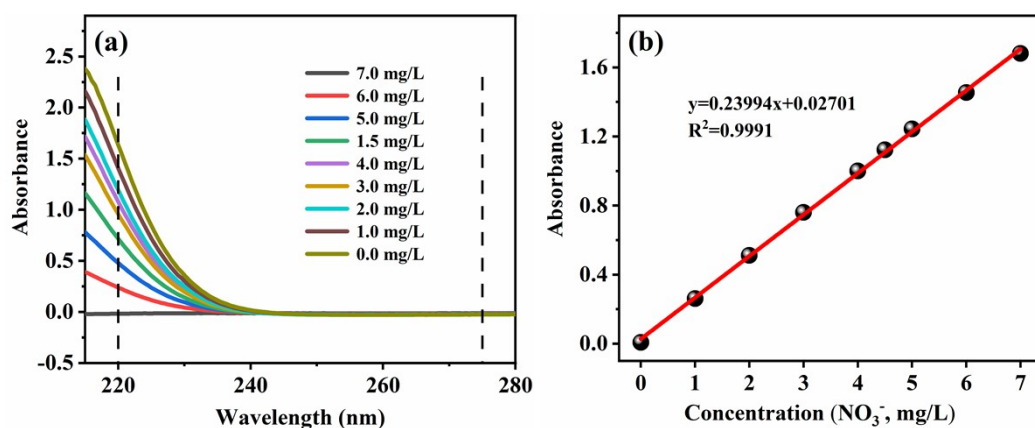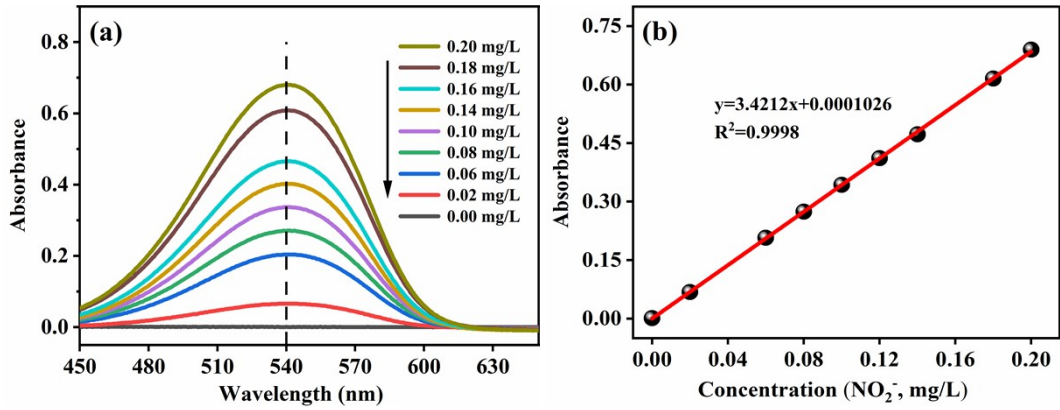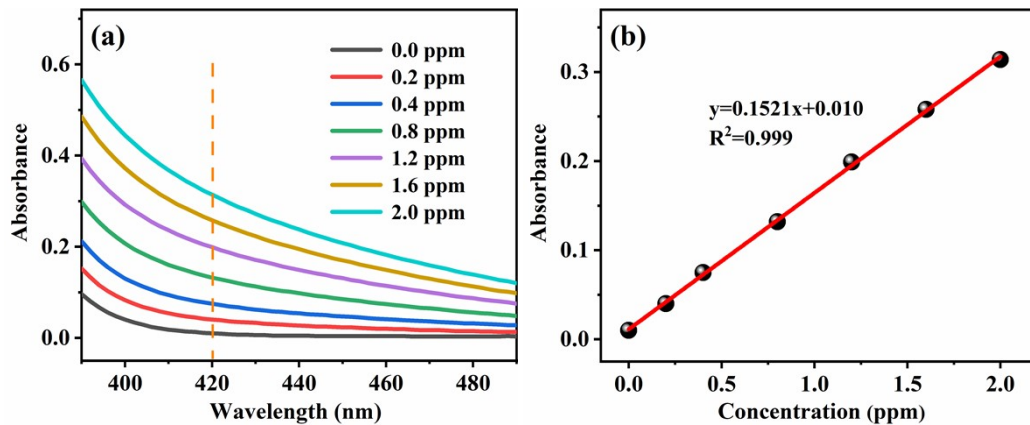

Figure S3. (a) UV-Vis absorption curves of Nessler's reagent assays kept with different concentrations of NH_4^+-N. (b) Calibration curve used to estimate the concentrations of NH_4^+-N.

1.4 Calculations of FE, NH₃ yield, selectivity and conversion rate

$$FE = \left(8 \times F \times C_{NH_3} \times V\right) \div \left(M_{NH_3} \times Q\right) \times 100\%$$

$$NH_3 \ yield = \left(C_{NH_3} \times V\right) \div \left(M_{NH_3} \times t \times S\right)$$

$$S_{NH_3} = C_{NH_3} \div \Delta C_{NO_3^-} \times 100\%$$

$$Conversion = \Delta C_{NO_3^-} \div C_0 \times 100\%$$

Where F is the Faradic constant (96485 C mol^{-1}), C_{NH3} is the measured NH$_3$ concentration, V is the volume of electrolyte in the anode compartment (120 mL), M_{NH3} is the molar mass of NH$_3$, Q is the total quantity of applied electricity, t is the electrolysis time (1 h), S is the loaded area of catalyst (1 cm^{-2}), C_0 is the initial concentration of NO$_3^-$, and ΔC_{NO3^-} is the concentration difference of NO$_3^-$ before and after electrolysis.

1.5 Electrochemical *in-situ* ATR-FTIR test

The glassy carbon electrode supported by catalyst was used as the working electrode. 0.1 M Na$_2$SO$_4$ with 50 ppm NO$_3^-$-N was adopted as the electrolyte. The *in-situ* ATR-FTIR spectra were collected during LSV test from 0 to -1.5 V vs. Ag/AgCl with a scan rate of 2 mV/s. Each reflectance spectrum was collected with a time resolution of 60 s at a spectral resolution of 4 cm^{-1}. Then, all of the spectra were transformed into absorbance spectra.
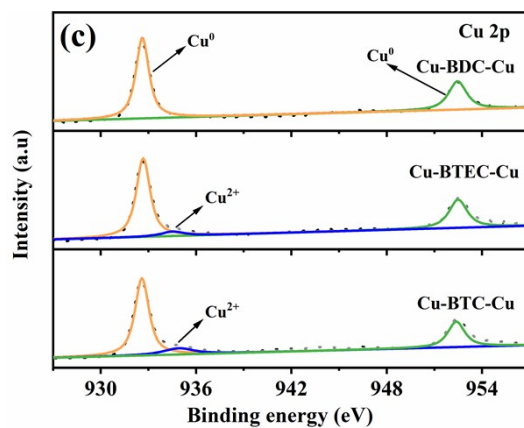
2. Result and discussion
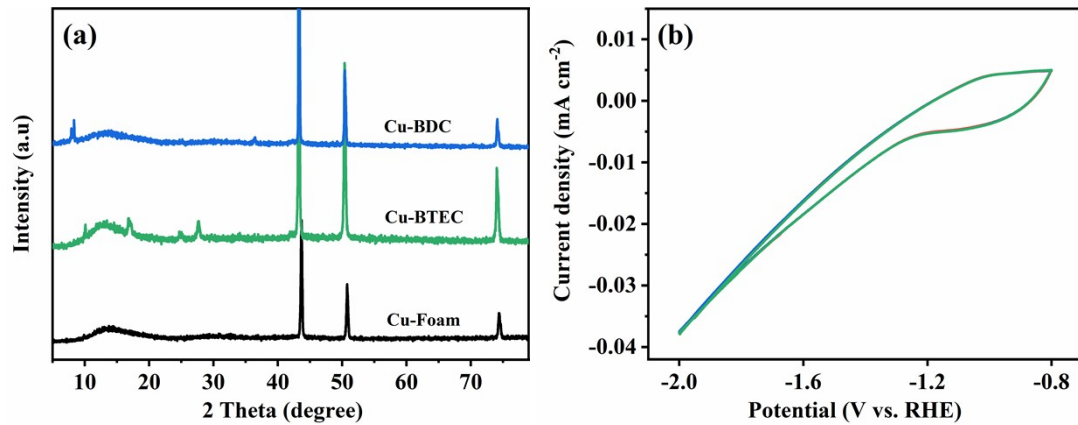
Figure S4. (a) XRD patterns of the Cu-BTC, Cu-BTEC and Cu-BDC. (b) CV curves of Cu-BTC in the reduction process during the last few cycles. (c) High-resolution XPS spectra for Cu 2p of the Cu-BTC-Cu, Cu-BTEC-Cu, and Cu-BDC-Cu.
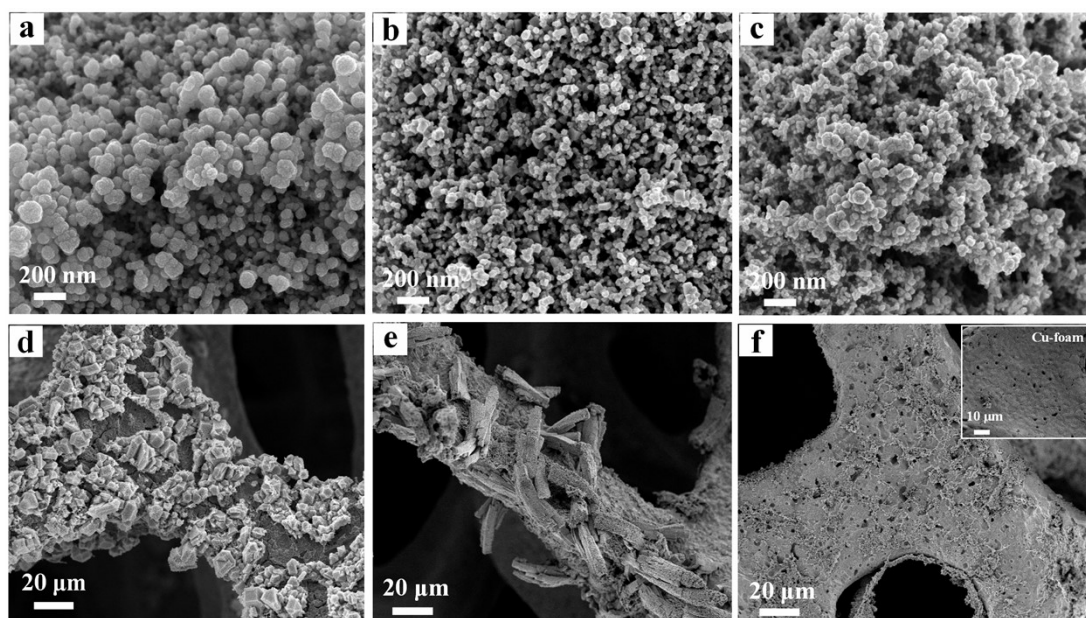
Figure S5. SEM images of the (a, d) Cu-BTC-Cu, (b, e) Cu-BTEC-Cu, and (c, f) Cu-BDC-Cu.

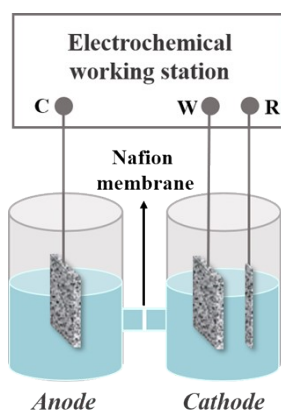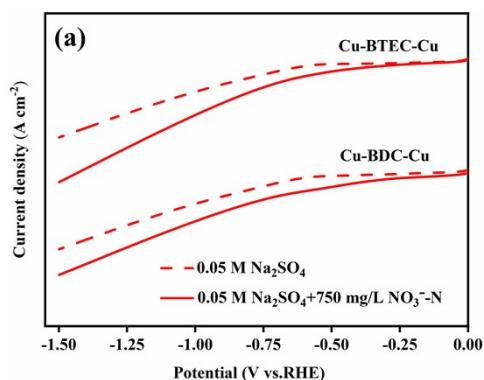**Figure S7**. (a) LSV curves of Cu-BTEC-Cu and Cu-BDC-Cu at 0.05 M Na_2SO_4 and 0.05 M Na_2SO_4+750 mg/L NO_3^--N.
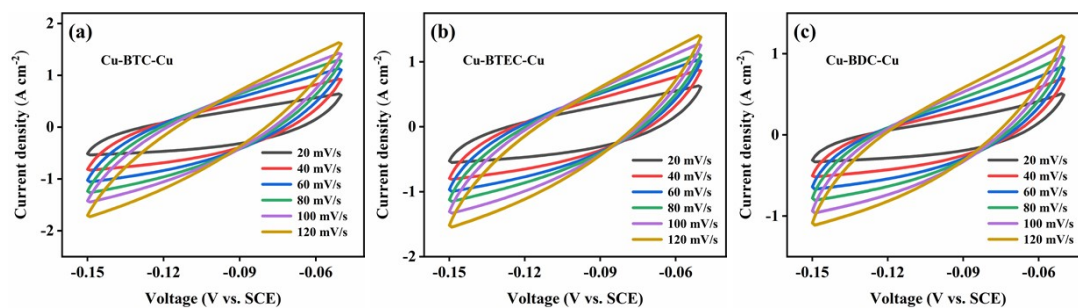
Figure S8. CV curves of (a) Cu-BTC-Cu, (b) Cu-BTEC-Cu, and (c) Cu-BDC-Cu under different scan rates from 20 to 120 mV S^{-1}
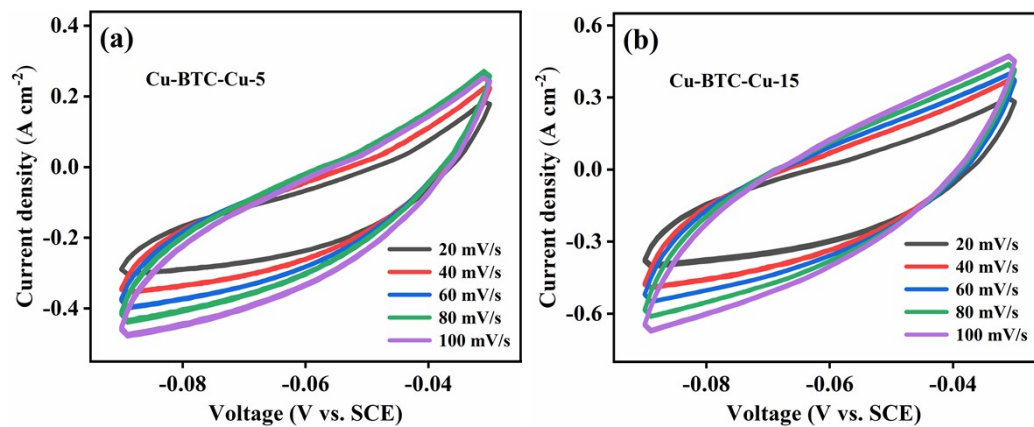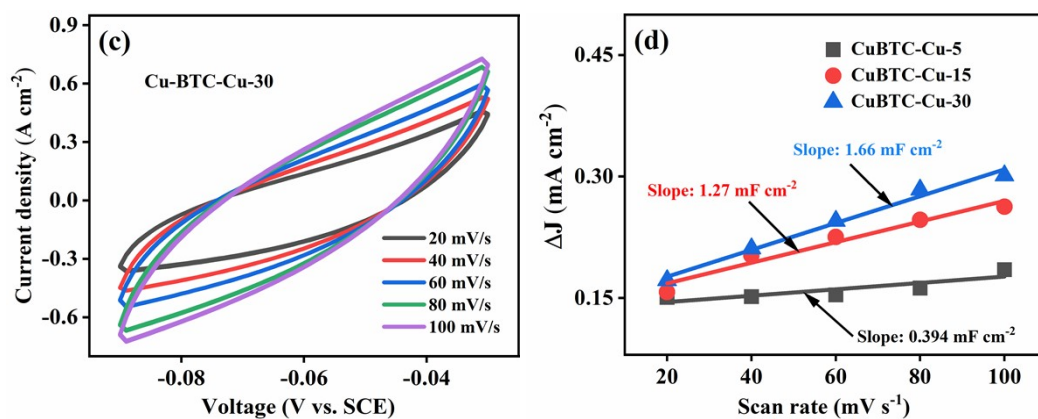
Figure S9. CV curves of (a) Cu-BTC-Cu-5, (b) Cu-BTEC-Cu-15, and (c) Cu-BDC-Cu-30 under different scan rates from 20 to 100 mV S^{-1}. (d) The fitted linear relationship between current density and the scan rate for the Cu-BTC-Cu-5, Cu-BTEC-Cu-15, and Cu-BDC-Cu-30.
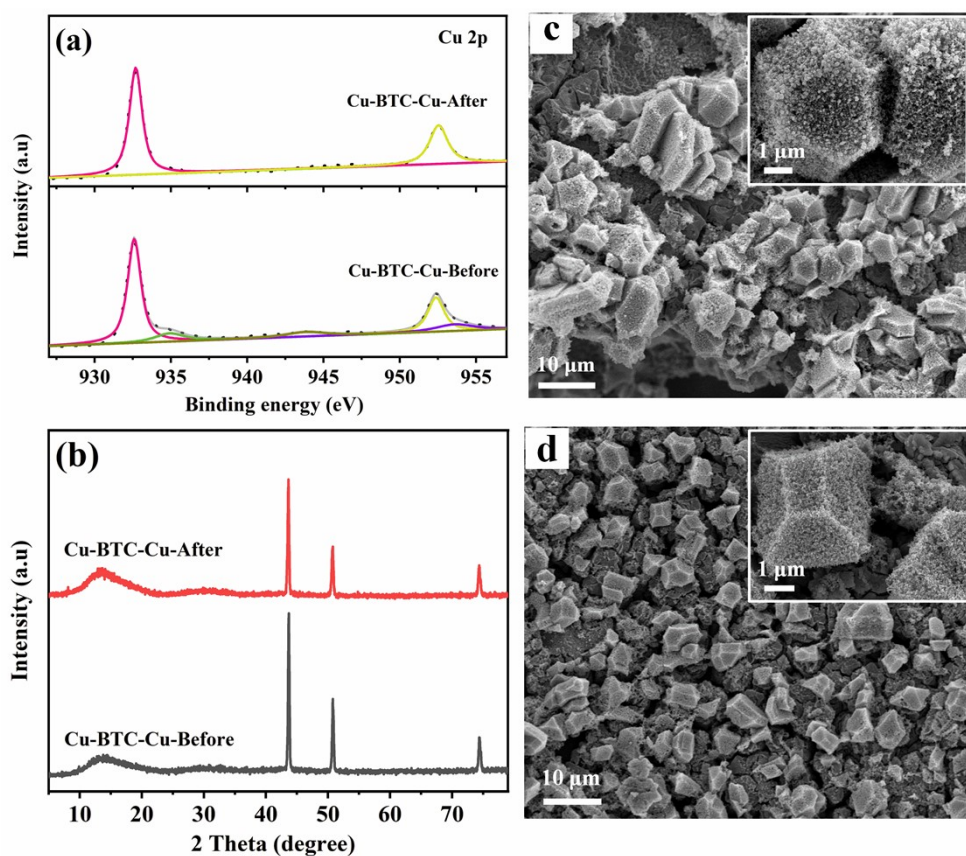
Figure S10. Characterizations of the Cu-BTC-Cu participates in electrocatalytic nitrate reduction before and after (Cu-BTC-Cu-Before and Cu-BTC-Cu-After): (a) High-resolution XPS spectra for Cu 2p, (b) XRD patterns, and (c, d) SEM images.

The standard curve is prepared by external standard method using NH$_4$Cl as standard solution. (Figure S11 a and b)
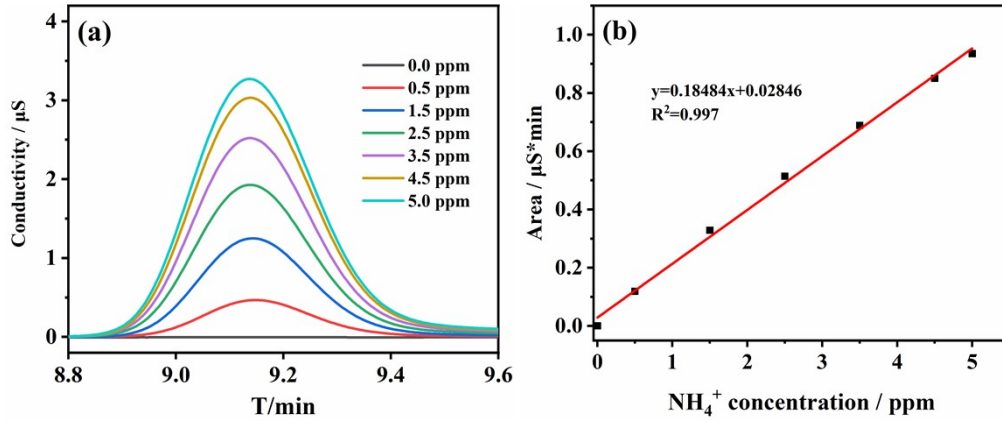
Figure S11. The NH_4^+ detection of (a) standard spectra and (b) fitting curve by ion chromatography.
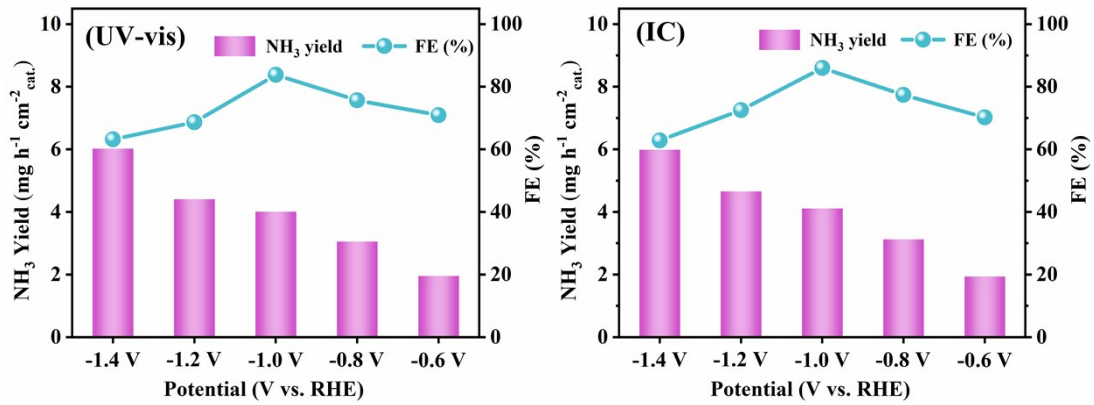
Figure S12. NH_3 yields and FE of the Cu-BTC-Cu at different potentials by the Nessler's color reagent and ion chromatography.
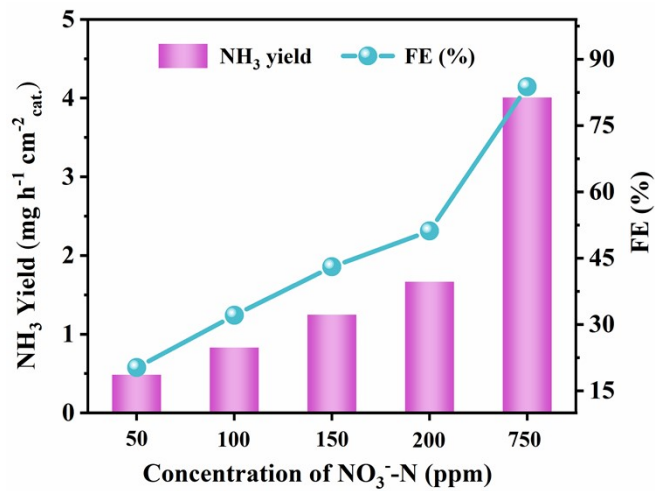
Figure S13. NH_3 yields and FE of the Cu-BTC-Cu at different concentrations of NO_3^--N.
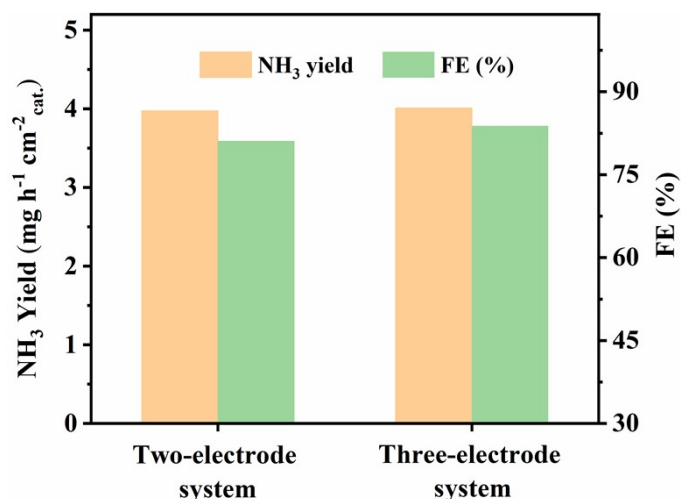
Figure S14. NH_3 yields and FE of the Cu-BTC-Cu at two-electrode and three-electrode system.
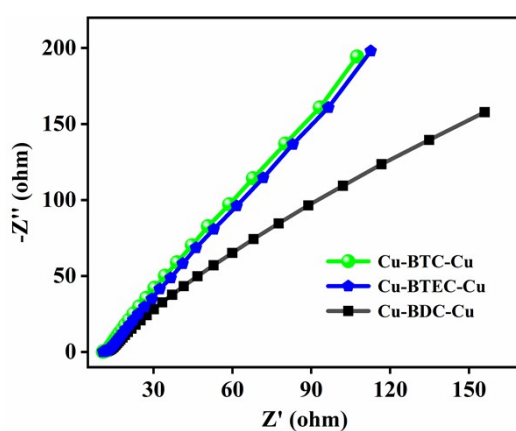
Figure S15. The electrochemical impedance spectroscopy of Cu-BTC-Cu, Cu-BTEC-Cu, and Cu-BDC-Cu

Table S1 Comparison of ammonia synthesis from nitrate reduction over Cu-BTC-Cu and other reported catalysts.

| Catalyst	Electrolyte	NH_3 yield （$\mu g\ h^{-1}\ cm^{-2}$）	Ref.
Cu-BTC-Cu	0.05 M K_2SO_4/750 mg L^{-1} NO_3^--N	4009.3	This work
Cu@Th-BPYDC	1 M KOH/1400 mg L^{-1} NO_3^--N	3830.1	[1]
BCN-Cu 10	0.1 M KOH/1400 mg L^{-1} NO_3^--N	1900.07	[2]
FeS_2/RGO	0.5 M Na_2SO_4/1400 mg L^{-1} NO_3^--N	2320	[3]
WSe_{2-x}	0.5 M Na_2SO_4/1400 mg L^{-1} NO_3^--N	2420	[4]
MnO_{2-x}	0.1 M Na_2SO_4/1400 mg L^{-1} NO_3^--N	3340	[5]
BCN@Ni	0.1 M KOH/1400 mg L^{-1} NO_3^--N	2320.2	[6]

Pd/TiO$_2$	1 M LiCl/3500 mg L^{-1} NO$_3^-$-N	1120	[7]
BP	0.5 M Na$_2$SO$_4$/1400 mg L^{-1} NO$_3^-$-N	3100	[8]
FeOOH	0.1 M PBS/0.1 M NaNO$_3$	2419	[9]
Co$_3$O$_4$-Mn$_2$	0.5 M K$_2$SO$_4$/1400 mg L^{-1} NO$_3^-$-N	3500	[10]
Fe-MoS$_2$	0.1 M Na$_2$SO$_4$+0.1 M NaOH/0.1 M NaNO$_3$	510	[11]
MoO$_2$-C NBF	1 M KOH/1400 mg L^{-1} NO$_3^-$-N	1857.7	[12]

References:

(1) Gao, Z.; Lai, Y.; Tao, Y.; Xiao, L.; Zhang, L.; Luo, F. Constructing Well-Defined and Robust Th-MOF-Supported Single-Site Copper for Production and Storage of Ammonia from Electroreduction of Nitrate. *ACS Cent Sci* **2021**, *7* (6), 1066-1072. DOI: 10.1021/acscentsci.1c00370.

(2) Zhao, X.; Jia, X.; He, Y.; Zhang, H.; Zhou, X.; Zhang, H.; Zhang, S.; Dong, Y.; Hu, X.; Kuklin, A. V.; et al. Two-dimensional BCN matrix inlaid with single-atom-Cu driven electrochemical nitrate reduction reaction to achieve sustainable industrial-grade production of ammonia. *Applied Materials Today* **2021**, *25*. DOI: 10.1016/j.apmt.2021.101206.

(3) Zhang, N.; Zhang, G.; Tian, Y.; Tang, Y.; Chu, K. FeS_2 nanoparticles on reduced graphene oxide: an efficient electrocatalyst for nitrate electroreduction to ammonia. *Dalton Trans* **2022**, *51* (44), 16805-16810. DOI: 10.1039/d2dt02991j.

(4) Shen, P.; Wang, G.; Chen, K.; Kang, J.; Ma, D.; Chu, K. Selenium-vacancy-rich WSe_2 for nitrate electroreduction to ammonia. *J Colloid Interface Sci* **2023**, *629* (Pt A), 563-570. DOI: 10.1016/j.jcis.2022.09.012.

(5) Wang, G.; Shen, P.; Luo, Y.; Li, X.; Li, X.; Chu, K. A vacancy engineered MnO_{2-x} electrocatalyst promotes nitrate electroreduction to ammonia. *Dalton Trans* **2022**, *51* (24), 9206-9212. DOI: 10.1039/d2dt01431a.

(6) Zhao, X.; Zhu, Z.; He, Y.; Zhang, H.; Zhou, X.; Hu, W.; Li, M.; Zhang, S.; Dong, Y.; Hu, X.; et al. Simultaneous anchoring of Ni nanoparticles and single-atom Ni on BCN matrix promotes efficient conversion of nitrate in water into high-value-added ammonia. *Chemical Engineering Journal* **2022**, *433*. DOI: 10.1016/j.cej.2021.133190.

(7) Guo, Y.; Zhang, R.; Zhang, S.; Zhao, Y.; Yang, Q.; Huang, Z.; Dong, B.; Zhi, C. Pd doping-weakened intermediate adsorption to promote electrocatalytic nitrate reduction on TiO_2 nanoarrays for ammonia production and energy supply with zinc–nitrate batteries. *Energy & Environmental Science* **2021**, *14* (7), 3938-3944. DOI: 10.1039/d1ee00806d.

(8) Zhang, N.; Zhang, G.; Tian, Y.; Guo, Y.; Chu, K. Boron phosphide as an efficient metal-free catalyst for nitrate electroreduction to ammonia. *Dalton Trans* **2023**, *52* (14), 4290-4295. DOI: 10.1039/d3dt00551h.

(9) Liu, Q.; Liu, Q.; Xie, L.; Ji, Y.; Li, T.; Zhang, B.; Li, N.; Tang, B.; Liu, Y.; Gao, S.; et al. High-Performance Electrochemical Nitrate Reduction to Ammonia under Ambient Conditions Using a FeOOH Nanorod Catalyst. *ACS Appl Mater Interfaces* **2022**, *14* (15), 17312-17318. DOI: 10.1021/acsami.2c00436.

(10) Liu, D.; Qiao, L.; Chen, Y.; Zhou, P.; Feng, J.; Leong, C. C.; Ng, K. W.; Peng, S.; Wang, S.; Ip, W. F.; et al. Electrocatalytic reduction of nitrate to ammonia on low-cost manganese-incorporated Co_3O_4 nanotubes. *Applied Catalysis B: Environmental* **2023**, *324*. DOI:

10.1016/j.apcatb.2022.122293.

(11) Li, J.; Zhang, Y.; Liu, C.; Zheng, L.; Petit, E.; Qi, K.; Zhang, Y.; Wu, H.; Wang, W.; Tiberj, A.; et al. 3.4% Solar-to-Ammonia Efficiency from Nitrate Using Fe Single Atomic Catalyst Supported on MoS$_2$ Nanosheets. *Advanced Functional Materials* **2021**, *32* (18). DOI: 10.1002/adfm.202108316.

(12) Yan, J.; Liu, P.; Li, J.; Huang, H.; Song, W. Effect of valence state on electrochemical nitrate reduction to ammonia in molybdenum catalysts. *Chemical Engineering Journal* **2023**, *459*. DOI: 10.1016/j.cej.2023.141601.